

# A New Superionic Plastic Polymorph of the Na<sup>+</sup> Conductor Na<sub>3</sub>PS<sub>4</sub>

Theodosios Famprikis,<sup>\*,†,‡,§,¶</sup> James A. Dawson,<sup>‡,§,¶</sup> François Fauth,<sup>||,¶</sup> Oliver Clemens,<sup>⊥,¶</sup> Emmanuelle Suard,<sup>#</sup> Benoit Fleutot,<sup>†</sup> Matthieu Courty,<sup>†</sup> Jean-Noël Chotard,<sup>†,¶</sup> M. Saiful Islam,<sup>\*,†,§,¶</sup> and Christian Masquelier<sup>\*,†,§,∇,¶</sup>

<sup>†</sup>Laboratoire de Réactivité et Chimie des Solides (CNRS UMR 7314), Amiens, France

<sup>‡</sup>Department of Chemistry, University of Bath, Bath, United Kingdom

<sup>§</sup>ALISTORE–European Research Institute (CNRS FR 3104), Amiens, France

<sup>||</sup>CELLS–ALBA Synchrotron, Barcelona, Spain

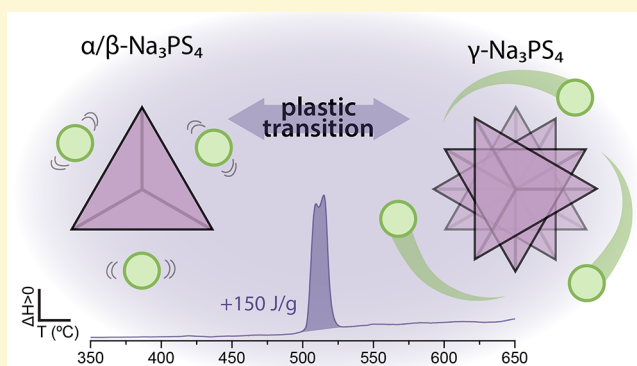
<sup>⊥</sup>Fachgebiet Materialdesign durch Synthese, Institut für Materialwissenschaft, Technische Universität Darmstadt, and Karlsruher Institut für Technologie, Institut für Nanotechnologie, Karlsruhe, Germany

<sup>#</sup>Institut Laue–Langevin, Grenoble, France

<sup>∇</sup>Réseau sur le Stockage Electrochimique de l'Énergie (RS2E CNRS FR 3459), Amiens, France

## Supporting Information

**ABSTRACT:** Na<sub>3</sub>PS<sub>4</sub> is one of the most promising Na<sup>+</sup> conductors, relevant for applications that can leverage its high ionic conductivity, such as solid-state batteries. Currently, two crystalline phases of the material have been identified, and it has been thought to melt above 500 °C. In contrast, based on diffraction, ab initio simulations, impedance spectroscopy, and thermal analysis, we show that Na<sub>3</sub>PS<sub>4</sub> remains solid above this temperature and transforms to a third polymorph, γ, exhibiting fast-ion conduction and an orthorhombic crystal structure. We show that the fast Na<sup>+</sup>-conduction is associated with rotational motion of the thiophosphate polyanions pointing to a plastic crystal. These findings are of major importance for the development and understanding of new polyanion-based solid electrolytes.



Sodium thio-orthophosphate (Na<sub>3</sub>PS<sub>4</sub>) has received considerable attention as a solid electrolyte material, especially for the development of sodium solid-state batteries.<sup>1</sup> Its crystalline structure and Na<sup>+</sup> ion-conduction properties were first explored by Jansen and Henseler and two polymorphs are currently known: the room-temperature tetragonal form (α), which transforms to a closely related cubic form (β) above 261 °C.<sup>2</sup> The ionic conductivity of crystalline Na<sub>3</sub>PS<sub>4</sub> prepared by solid-state synthesis is of the order of 10<sup>-6</sup>–10<sup>-5</sup> S/cm at 298 K,<sup>2–4</sup> which limits its applicability to bulk solid-state battery applications.

A resurgence in interest in Na<sub>3</sub>PS<sub>4</sub> came as a result of an improvement of its ionic conductivity achieved through mechanochemical synthesis, first reported by Hayashi et al.<sup>5,6</sup> Such ball-milled, “glass-ceramic” Na<sub>3</sub>PS<sub>4</sub> exhibits ambient ionic conductivities on the order of 10<sup>-4</sup> S/cm,<sup>3–7</sup> enabling its incorporation in solid-state batteries.<sup>5–11</sup> The mechanochemical route is thought to stabilize the cubic polymorph (β), as

observed by Bragg diffraction, but there exist conflicting reports regarding its local and average structure.<sup>3,10,12</sup> In addition, Jansen and Henseler hypothesized a pre-melting phase transition to a third phase, associated with rotational mobility of the PS<sub>4</sub><sup>3-</sup> tetrahedra, which they were, however, unable to substantiate.<sup>2</sup> Such materials possessing significant rotational, conformational, and/or translational mobility of their constituent atoms, in combination with long-range order (crystallinity), are referred to as plastic crystals, with properties between those of classical liquids and solids.

These unanswered questions regarding the structure of Na<sub>3</sub>PS<sub>4</sub> motivated us to pursue thorough investigations of the effect of its microstructure on ion conduction,<sup>13</sup> as well as the evolution of its crystalline structure and electrical properties

Received: August 12, 2019

Accepted: October 30, 2019

Published: October 30, 2019

with temperature. We report here the observation of a previously unknown phase, which we attribute to a third polymorph of  $\text{Na}_3\text{PS}_4$  that exhibits fast  $\text{Na}^+$  conduction and plastic crystal characteristics, including rotational motion of the  $\text{PS}_4^{3-}$  anions.<sup>14–16</sup>

First, we performed temperature-controlled synchrotron X-ray diffraction (XRD) experiments, which yielded results in agreement with published literature up to 500 °C, as shown in the contour plot of Figure 1a. The tetragonal polymorph ( $\alpha$ -

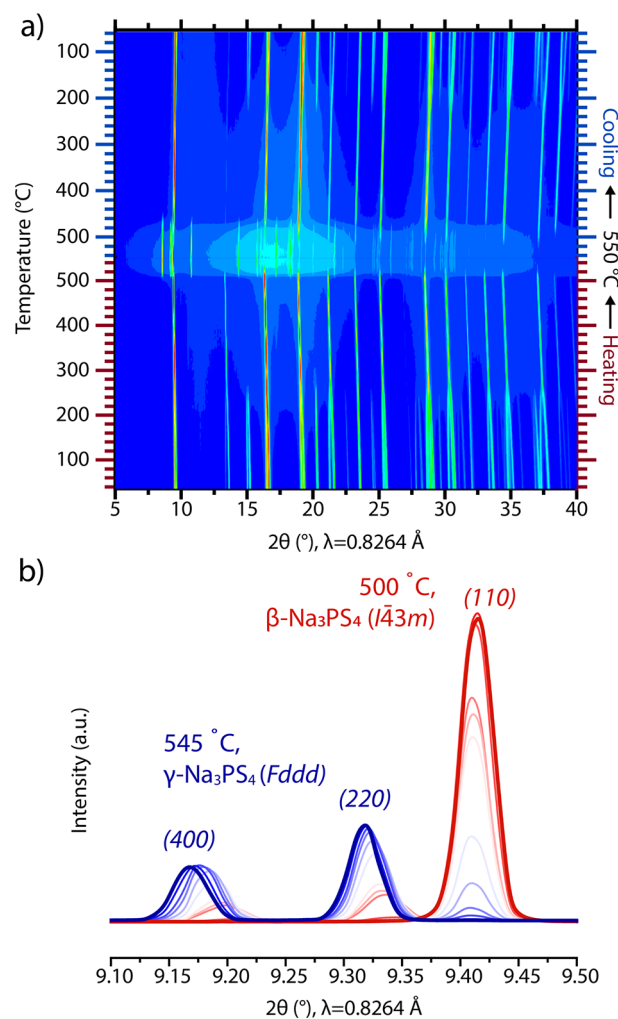


**Figure 1.** Temperature-controlled synchrotron X-ray diffraction (XRD) of  $\text{Na}_3\text{PS}_4$ : (a) logarithmic contour plot of diffractograms in the range of 30–550 °C upon heating and cooling (the color code, from blue to red, indicates the range from low diffraction intensity to high diffraction intensity, respectively); (b) superimposed sections of the diffractograms at  $9.1^\circ < 2\theta < 9.5^\circ$  and  $500^\circ\text{C} < T < 545^\circ\text{C}$  every 5 °C.

$\text{Na}_3\text{PS}_4$ ) is observed at 25 °C and persists with heating up to 220 °C when it begins transforming to the cubic polymorph ( $\beta$ - $\text{Na}_3\text{PS}_4$ ); the transformation reaches completion at 275 °C. In turn, the diffraction peaks of  $\beta$ - $\text{Na}_3\text{PS}_4$  are observable until 500 °C.

Above 500 °C, new diffraction peaks appear, indicating the formation of another crystalline phase. Gradually, the intensities of the peaks attributed to  $\beta$ - $\text{Na}_3\text{PS}_4$  decrease and those of the new phase increase (Figure 1b). The transformation is complete at 545 °C and is accompanied by a

distinct wavelike rise in the baseline diffraction signal, typically associated with the diffuse scattering from amorphous or liquid samples.

Upon subsequent cooling, the crystallographic transformations are reversible with the reappearance of  $\beta$ - and  $\alpha$ - $\text{Na}_3\text{PS}_4$ , respectively. Neutron diffraction experiments are consistent with the XRD observations (see Figure S1 in the Supporting Information), showing the same phase evolution with temperature, despite the stark differences in sample environment ( $\sim 2$  g of sample in vanadium container under secondary vacuum for neutrons;  $\sim 10$  mg of sample in sealed quartz ampule under positive pressure of argon for synchrotron). These observations lead to the conclusion of the existence of a third polymorph of  $\text{Na}_3\text{PS}_4$ , accessible above 500 °C, which we will refer to as  $\gamma$ .

The XRD pattern of  $\gamma$ - $\text{Na}_3\text{PS}_4$  can be fully indexed in an orthorhombic  $Fddd$  space group with lattice parameters of 6.6055(1), 11.7143(2), and 20.7378(3) Å at 550 °C (Figure 2). The  $\beta \rightarrow \gamma$  transition is accompanied by an abrupt increase in the volume of the unit cell by  $\sim 10\%$ , from 180.8 Å<sup>3</sup>/f.u. to 198.8 Å<sup>3</sup>/f.u. (assuming  $Z = 8$  for the orthorhombic cell). A direct structural solution of the  $\gamma$ -phase from the powder diffractogram is complicated by diffuse electronic density attesting to extensive disorder and by an apparent effect of preferential orientation: the relative intensities for the  $\alpha$ - and  $\beta$ -phases are different on heating and cooling, respectively (see Figure 1a).

Based on the observed space group and mapping of the scattering (electronic) density of the high-temperature diffractograms, we deduce that the  $\gamma$ -phase is structurally related to thenardite ( $\text{Na}_2\text{SO}_4$ ), which also crystallizes in  $Fddd$  (albeit with a much smaller unit cell). Using the structure of  $\text{Na}_2\text{SO}_4$  as a starting point, we expanded its unit cell to our observed lattice parameters and replaced  $\text{SO}_4^{2-}$  tetrahedra with  $\text{PS}_4^{3-}$  to reach a hypothetical “ $\text{Na}_2\text{PS}_4$ ” structure (see Figure S2 in the Supporting Information). This treatment resulted directly in realistic P–S bond length, close to 2 Å, thereby validating the approach.

We then performed static density functional theory (DFT) calculations to attempt to locate the additional Na position(s). The expansion of the thenardite unit cell from  $\text{Na}_2\text{SO}_4$  to  $\gamma$ - $\text{Na}_3\text{PS}_4$  creates ample “interstitial” space for Na around the structure-forming tetrahedra. Indeed, our simulation analysis resulted in multiple structures with varying Na positions but very close energetically (within 15 meV/atom), indicating a high level of disorder of Na atoms among multiple positions. When relaxed, these structures all present formation energies only slightly higher ( $< 70$  meV/atom) than the cubic  $\beta$ -phase. This difference is very small considering that the true average structure would feature partially occupied atoms, and it is also reasonable to expect high entropic contributions from pronounced atomic mobilities. Both of the above effects are not explicitly captured in the static DFT calculations and result in an overestimation of the free energy for the  $\gamma$ -phase.<sup>17</sup>

Combining the multiple possible positions for Na determined above, we propose an approximate crystal structure for  $\gamma$ - $\text{Na}_3\text{PS}_4$ , shown in Figure 3. This rigid model can still not fully explain the diffractogram, because it corresponds to a single conformation of the  $\text{PS}_4^{3-}$  tetrahedra and is constrained by the  $Fddd$  long-range symmetry. Instead, our ab initio simulations and scattering density mapping show two features: (i) multiple S positions are possible around the central P atom (i.e., multiple conformations of the  $\text{PS}_4^{3-}$  tetrahedra, each

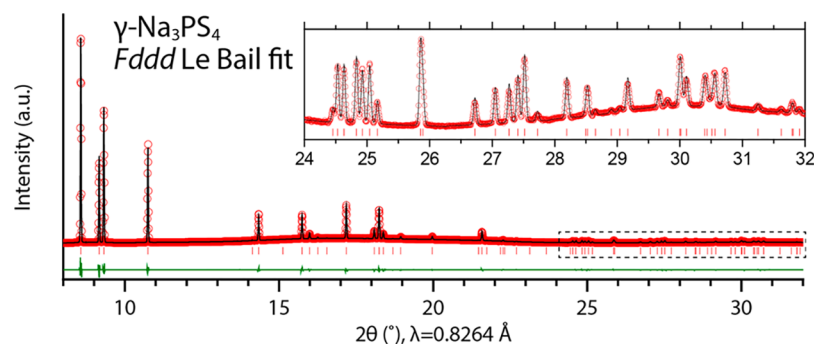


Figure 2. Le Bail (profile) fit of the synchrotron X-ray diffractogram of  $\text{Na}_3\text{PS}_4$  at 550 °C.

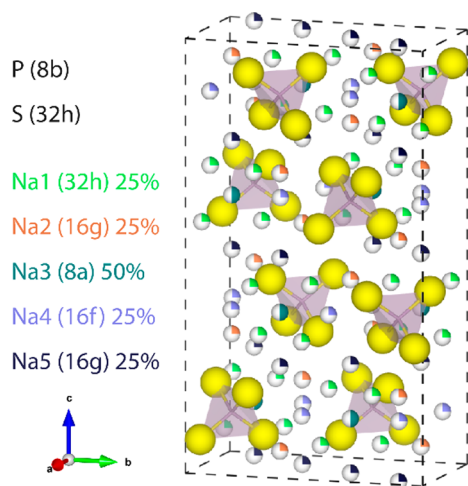


Figure 3. Proposed structure of  $\gamma\text{-Na}_3\text{PS}_4$  from static *ab initio* calculations. P and S in purple and yellow, respectively, were fixed into perfect  $\text{PS}_4^{3-}$  tetrahedra. Relative occupations of Na sites were approximated from the relative calculated energies of different configurations. Crystallographic information file (.cif) provided as Supporting Information.

surrounded by its associated stable Na positions), and (ii) these are not locally constrained by the long-range symmetry. Diffraction probes an average structure; i.e., a superposition of all different possible conformations of  $\text{PS}_4^{3-}$  and further analysis of the diffuse scattering is needed to unambiguously elucidate the complete average structure. We present our attempts to that end and propose a preliminary structure solution consistent with both the diffractogram and the DFT calculations in the Supporting Information (Figures S3 and S4).

Differential scanning calorimetry (DSC) data, shown in Figure 4a and performed at the same heating rate as the diffraction experiments (5 °C/min), correspond well with the observed diffraction behavior and previous differential thermal analysis results.<sup>2</sup> No thermal signature is observed for the  $\alpha \rightarrow \beta$  phase transition, consistent with the very small difference in formation energy between the two polymorphs, amounting to  $\sim 5$  meV/atom, as calculated by DFT,<sup>12,18,19</sup> and with the minor atomic rearrangements required for this transition.

In contrast, an intense doublet thermal signature is observed upon heating, centered at 509.5 and 515 °C with an onset at 503.5 °C, collectively amounting to  $\sim 150$  J/g. Jansen and Henseler, who also observed this doublet, attributed it to pre-melting and melting.<sup>2</sup> Their assignment was likely based on earlier investigations of the  $\text{Na}_2\text{S}\text{-P}_2\text{S}_5$  phase diagram, which

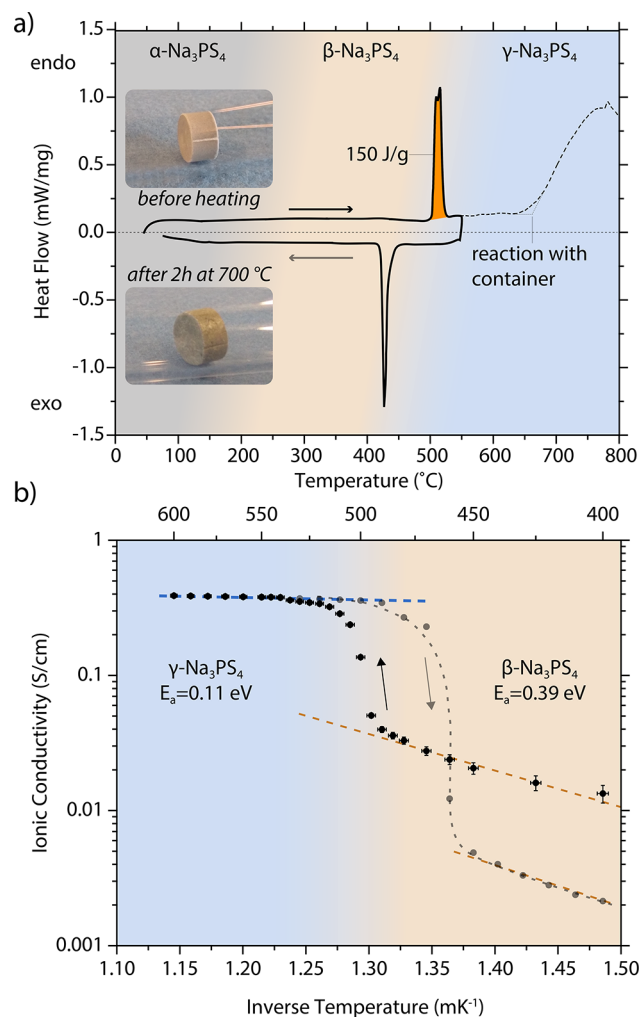
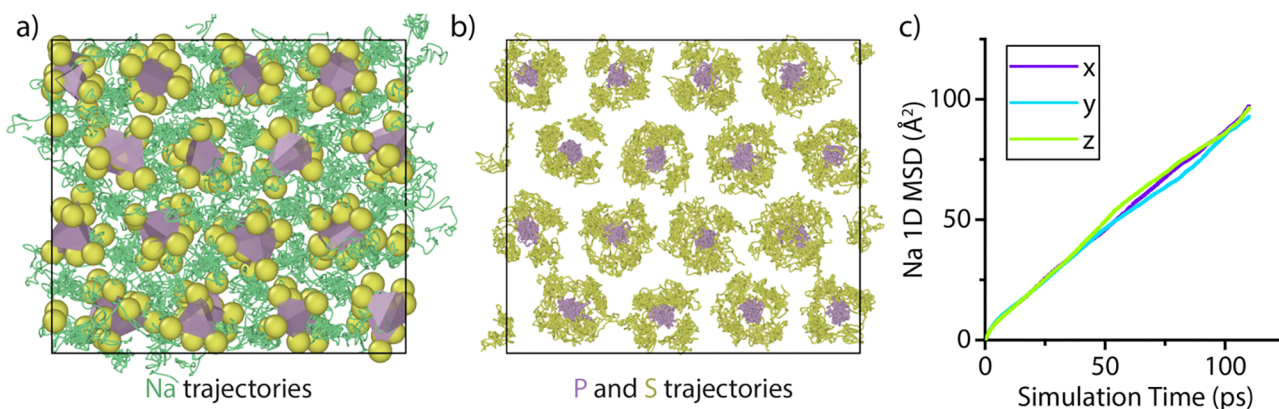


Figure 4. (a) Differential scanning calorimetry (DSC) curve of  $\text{Na}_3\text{PS}_4$  (inset shows photographs of  $\text{Na}_3\text{PS}_4$  pellets before and after heating to 550 °C for 2 h). (b) Evolution of ionic conductivity in  $\text{Na}_3\text{PS}_4$ , as measured by impedance spectroscopy.

had proposed a melting point of 790 K (517 °C) for  $\text{Na}_3\text{PS}_4$ .<sup>20</sup> Interestingly, the same authors reported on the “mechanical stability” of pelletized  $\text{Na}_3\text{PS}_4$  up to and above the reported melting point of 517 °C. Indeed, we confirm that pellets of  $\text{Na}_3\text{PS}_4$  maintain their shape after 2 h at 700 °C, significantly above the proposed melting temperature (Figure 4a, inset). In attempting to determine the actual melting point through DSC, a further broad endothermic effect was observed with an onset of 661.7 °C. We associate the latter with reactivity of  $\gamma$



**Figure 5.** Atomic mobility results from ab initio molecular dynamics of  $\gamma$ - $\text{Na}_3\text{PS}_4$ . Atomic trajectories of (a) Na and (b) P and S (green, purple and yellow lines, respectively) shown in projection through the bc plane for 50 ps after equilibration of a 900 K simulation without extrinsic vacancies. (c)  $\text{Na}^+$  mean-squared displacements (MSD) in each spatial dimension.

$\text{Na}_3\text{PS}_4$  with the alumina sample container; given that pellets heated in quartz at 700 °C still maintain their shape (Figure 4a, inset) and orthorhombic diffraction characteristics (not shown). Thus, we associate the thermal effects at  $\sim 500$  °C with the  $\beta \rightarrow \gamma$  phase transition and re-evaluate the melting point of  $\text{Na}_3\text{PS}_4$  to  $>700$  °C. Furthermore, an increase in the DSC baseline allowed us to determine an increased heat capacity of the  $\gamma$ -phase (1.19 J/(g/K) at 550 °C), compared to that of the  $\alpha$ - and  $\beta$ -phases (1.03 J/(g/K) at 100 °C).

The ionic conductivity of the samples was extracted from impedance spectra measured as a function of temperature (see Figure S5 in the Supporting Information) and is presented in the Arrhenius plot of Figure 4b. For  $\beta$ - $\text{Na}_3\text{PS}_4$  (400–480 °C), we observe an activation energy of  $395 \pm 10$  meV, in good agreement with the value reported by Jansen and Henseler (402 meV).<sup>2</sup> The  $\beta \rightarrow \gamma$  transition at 500 °C causes a sudden increase in the ionic conductivity of  $\text{Na}_3\text{PS}_4$  of about an order of magnitude, from  $\sim 40$  mS/cm to  $\sim 400$  mS/cm. The activation energy for ion conduction in the  $\gamma$ -phase is evaluated as  $110 \pm 10$  meV. The electrical behavior is reversible with a hysteresis on cooling, consistent with diffraction and thermal analysis. The hysteresis is likely linked to kinetic limitations for the transformation back to the  $\beta$ -phase. Upon cooling, an order of magnitude decrease in absolute conductivity of the  $\beta$ -phase was observed, which could be ascribed to crystallographic texturation, as evident in the diffractograms of Figure 1a and the creation of porosity in the pellet upon the sudden, significant ( $\sim 10\%$ ) crystallographic contraction upon the  $\gamma \rightarrow \beta$  transition.

Extrapolating the high-temperature electrical behavior to room temperature, the conductivity of  $\gamma$ - $\text{Na}_3\text{PS}_4$  would be  $\sim 50$  mS/cm, significantly higher than any known solid electrolyte for Na or Li. Of course, exploitation of  $\gamma$ - $\text{Na}_3\text{PS}_4$  for room-temperature applications, such as solid-state batteries, would necessitate its stabilization at lower temperatures than those presented here. Quenching<sup>21</sup> and/or chemical substitutions (e.g. Cl doping or polyanion mixing)<sup>18,22–29</sup> might prove useful to that effect, similar to what has been observed, for example, in analogous borohydride plastic crystal electrolytes.<sup>30–33</sup> The results of our preliminary unsuccessful efforts are outlined in the Supporting Information (Figure S6).

We further probed the atomic-scale ionic diffusion characteristics of the  $\gamma$ -phase by means of ab initio molecular dynamics (MD) simulations for a range of temperatures (600–1050 K), using, as a starting point, the derived thenardite structure

(Figure 3). The atomic trajectories show clear signs of fast ion conduction, with delocalized  $\text{Na}^+$  ions attesting to the effective “melting” of the Na sublattice (see Figure 5a). All  $\text{Na}^+$  ions are mobile, with some notable long-range displacements across the simulation cell, indicative of fast ion conduction. The  $\text{Na}^+$ -ion translational mobility is accompanied by distinct motion of the S atoms about the central P atoms of the thiophosphate tetrahedra (see Figure 5b). Despite their rotational motion, the (barycenters of the)  $\text{PS}_4^{3-}$  units remain translationally fixed to their starting position, confirming the macroscopically solid nature of the phase. The diffusion coefficients derived from the mean-squared displacement of the  $\text{Na}^+$  ions are approximately an order of magnitude higher than any previously calculated for the  $\beta$ - and  $\alpha$ -phases (shown in Figures S7 and S8 in the Supporting Information).<sup>18,19</sup> Furthermore, the calculated mean-squared displacements shown in Figure 5c show that the Na-ion diffusion is isotropic in three dimensions, despite the orthorhombic long-range symmetry. The calculated activation energy for Na diffusion is  $161 \pm 13$  meV, in good agreement with the values extracted from impedance spectroscopy.

The ensemble of our observations points to a plastic nature<sup>34–36</sup> for the  $\gamma$ - $\text{Na}_3\text{PS}_4$  phase, based on the following:

- The latent heat for the  $\beta \rightarrow \gamma$  transition is unusually high for a simple crystallographic phase transition. The measured value of 150 J/g (34.2 kJ/mol) is closer in magnitude to a typical heat of melting. Other known plastic phase transitions also exhibit such high latent heats, for example, 214 J/g (24.8 kJ/mol) for  $\text{Li}_2\text{SO}_4$  at 577 °C.<sup>37</sup> The increase of heat capacity upon the  $\beta \rightarrow \gamma$  transition is also consistent with the increased average kinetic energy of the atoms in  $\gamma$ - $\text{Na}_3\text{PS}_4$ .
- In the diffractograms of the  $\gamma$ -phase, the sharp Bragg peaks rapidly diminish in intensity at high angles and are accompanied by diffuse scattering. This is also a hallmark of plastic crystal phases, stemming from high mobility and short-range atomic correlations, also observable, e.g., in  $\text{Li}_2\text{SO}_4$ <sup>37</sup> and  $\text{LiCB}_{11}\text{H}_{12}$  and  $\text{NaCB}_{11}\text{H}_{12}$ .<sup>38</sup> Furthermore,  $\text{Li}_2\text{SO}_4$  also presents preferential orientation upon cooling from the plastic phase, similar to our observations for  $\text{Na}_3\text{PS}_4$  (Figure 1a).
- The measured ionic conductivity increases  $\sim 10$ -fold and the corresponding activation energy decreases sharply by

a factor of 4 upon transition from the  $\beta$ - to the  $\gamma$ - $\text{Na}_3\text{PS}_4$  phase.

- (d) There is a sizeable stepwise increase in unit-cell volume associated with the  $\beta \rightarrow \gamma$  transition, which is further correlated with the sharp increase in ionic conductivity. Such behavior has been observed in other fast-ion-conducting plastic crystal phases, e.g.,  $\text{Li}_2\text{SO}_4$  ( $\sim 3.2\%$  volume increase,<sup>39</sup> associated with one to four orders of magnitude conductivity increase<sup>40</sup> for the monoclinic to cubic transition at  $575\text{ }^\circ\text{C}$ <sup>41</sup>).
- (e) A distinct softening is evident when handling  $\text{Na}_3\text{PS}_4$  samples above  $500\text{ }^\circ\text{C}$ , which are very easily deformable under minimal pressure, attesting to the namesake of “plastic crystals”.<sup>42</sup>
- (f) Our MD simulations clearly demonstrate both fast  $\text{Na}^+$  conduction and  $\text{PS}_4^{3-}$  rotational motion.

In conclusion, we report a new polymorph ( $\gamma$ ) of  $\text{Na}_3\text{PS}_4$  with an orthorhombic crystal structure that exhibits fast ion conduction and plastic crystal characteristics. Our combined experimental and *ab initio* modelling investigation shows that isotropic  $\text{Na}^+$  conduction with a very low activation energy of  $\sim 0.1\text{ eV}$  is associated with rotational motion of the thiophosphate polyanions. Such concomitant motion could be a key factor in promoting high ionic conductivity and we believe that this study will stimulate further work on  $\gamma$ - $\text{Na}_3\text{PS}_4$  and plastic crystal solid electrolytes in general.

## ■ ASSOCIATED CONTENT

### ● Supporting Information

The Supporting Information is available free of charge on the ACS Publications website at DOI: [10.1021/acsmaterialslett.9b00322](https://doi.org/10.1021/acsmaterialslett.9b00322).

Approximate structure of  $\gamma$ - $\text{Na}_3\text{PS}_4$  from DFT calculations (CIF)

Approximate structure of  $\gamma$ - $\text{Na}_3\text{PS}_4$  from Rietveld refinements (CIF)

Experimental and computational methods and additional figures. (PDF)

## ■ AUTHOR INFORMATION

### Corresponding Authors

\*E-mail: [theo.famprakis@u-picardie.fr](mailto:theo.famprakis@u-picardie.fr) (T. Famprakis).

\*E-mail: [m.s.islam@bath.ac.uk](mailto:m.s.islam@bath.ac.uk) (M. S. Islam).

\*E-mail: [christian.masquelier@u-picardie.fr](mailto:christian.masquelier@u-picardie.fr) (C. Masquelier).

### ORCID

Theodosios Famprakis: [0000-0002-7946-1445](https://orcid.org/0000-0002-7946-1445)

James A. Dawson: [0000-0002-3946-5337](https://orcid.org/0000-0002-3946-5337)

François Fauth: [0000-0001-9465-3106](https://orcid.org/0000-0001-9465-3106)

Oliver Clemens: [0000-0002-0860-0911](https://orcid.org/0000-0002-0860-0911)

Jean-Noël Chotard: [0000-0002-9867-7954](https://orcid.org/0000-0002-9867-7954)

M. Saiful Islam: [0000-0003-3882-0285](https://orcid.org/0000-0003-3882-0285)

Christian Masquelier: [0000-0001-7289-1015](https://orcid.org/0000-0001-7289-1015)

### Author Contributions

T.F. coordinated the work, performed experiments, and prepared the manuscript. J.A.D. performed the *ab initio* calculations. F.F. performed the synchrotron diffraction experiments. E.S. assisted with the neutron diffraction. B.F. assisted with impedance spectroscopy. M.C. performed the thermal analysis. O.C. and J.-N.C. assisted with analysis of diffraction data. M.S.I. and C.M. supervised the work.

## Notes

The authors declare no competing financial interest.

## ■ ACKNOWLEDGMENTS

T.F. acknowledges the Alistore ERI and CNRS for their financial support in the form of a joint Ph.D. project between Amiens (France) and Bath (UK). M.S.I. and J.A.D. acknowledge the EPSRC Programme Grant (No. EP/M009521/1) and the MCC-Archer consortium (No. EP/L000202/1). The authors are indebted to A. Elbakyan for her invaluable help with the literature research.

## ■ REFERENCES

- (1) Famprakis, T.; Canepa, P.; Dawson, J. A.; Islam, M. S.; Masquelier, C. Fundamentals of Inorganic Solid-State Electrolytes for Batteries. *Nat. Mater.* **2019**, DOI: [10.1038/s41563-019-0431-3](https://doi.org/10.1038/s41563-019-0431-3)
- (2) Jansen, M.; Henseler, U. Synthesis, Structure Determination, and Ionic Conductivity of Sodium Tetrathiosphosphate. *J. Solid State Chem.* **1992**, *99*, 110–119.
- (3) Krauskopf, T.; Culver, S. P.; Zeier, W. G. Local Tetragonal Structure of the Cubic Superionic Conductor  $\text{Na}_3\text{PS}_4$ . *Inorg. Chem.* **2018**, *57*, 4739–4744.
- (4) Yu, C.; Ganapathy, S.; de Klerk, N. J. J.; van Eck, E. R. H.; Wagemaker, M. Na-Ion Dynamics in Tetragonal and Cubic  $\text{Na}_3\text{PS}_4$ , a Na-Ion Conductor for Solid State Na-Ion Batteries. *J. Mater. Chem. A* **2016**, *4*, 15095–15105.
- (5) Hayashi, A.; Noi, K.; Sakuda, A.; Tatsumisago, M. Superionic Glass-Ceramic Electrolytes for Room-Temperature Rechargeable Sodium Batteries. *Nat. Commun.* **2012**, *3*, 856.
- (6) Hayashi, A.; Noi, K.; Tanibata, N.; Nagao, M.; Tatsumisago, M. High Sodium Ion Conductivity of Glass–Ceramic Electrolytes with Cubic  $\text{Na}_3\text{PS}_4$ . *J. Power Sources* **2014**, *258*, 420–423.
- (7) Nguyen, H.; Banerjee, A.; Wang, X.; Tan, D.; Wu, E. A.; Doux, J.-M.; Stephens, R.; Verbist, G.; Meng, Y. S. Single-Step Synthesis of Highly Conductive  $\text{Na}_3\text{PS}_4$  Solid Electrolyte for Sodium All Solid-State Batteries. *J. Power Sources* **2019**, *435*, 126623.
- (8) Nagata, H.; Chikusa, Y. An All-Solid-State Sodium–Sulfur Battery Operating at Room Temperature Using a High-Sulfur-Content Positive Composite Electrode. *Chem. Lett.* **2014**, *43*, 1333–1334.
- (9) Tanibata, N.; Deguchi, M.; Hayashi, A.; Tatsumisago, M. All-Solid-State Na/S Batteries with a  $\text{Na}_3\text{PS}_4$  Electrolyte Operating at Room Temperature. *Chem. Mater.* **2017**, *29*, 5232–5238.
- (10) Hayashi, A.; Tatsumisago, M. *All-Solid-State Secondary Cell*. U.S. Patent No. 10,033,067, July 24, 2018.
- (11) Wan, H.; Mwizerwa, J. P.; Qi, X.; Xu, X.; Li, H.; Zhang, Q.; Cai, L.; Hu, Y.-S.; Yao, X. Nanoscaled  $\text{Na}_3\text{PS}_4$  Solid Electrolyte for All-Solid-State  $\text{FeS}_2/\text{Na}$  Batteries with Ultrahigh Initial Coulombic Efficiency of 95% and Excellent Cyclic Performances. *ACS Appl. Mater. Interfaces* **2018**, *10*, 12300–12304.
- (12) Nishimura, S.; Tanibata, N.; Hayashi, A.; Tatsumisago, M.; Yamada, A. The Crystal Structure and Sodium Disorder of High-Temperature Polymorph  $\beta$ - $\text{Na}_3\text{PS}_4$ . *J. Mater. Chem. A* **2017**, *5*, 25025–25030.
- (13) Dawson, J. A.; Canepa, P.; Clarke, M. J.; Famprakis, T.; Ghosh, D.; Islam, M. S. Toward Understanding the Different Influences of Grain Boundaries on Ion Transport in Sulfide and Oxide Solid Electrolytes. *Chem. Mater.* **2019**, *31*, 5296–5304.
- (14) Wilmer, D.; Feldmann, H.; Combet, J.; Lechner, R. E. Ion Conducting Rotor Phases—New Insights from Quasielastic Neutron Scattering. *Phys. B* **2001**, *301*, 99–104.
- (15) Witschas, M.; Eckert, H.; Wilmer, D.; Banhatti, R. D.; Funke, H.; Fitter, J.; Lechner, R. E.; Korus, G.; Jansen, M. Anion Rotation and Cation Transport in the Rotor Phase  $\alpha$ -Sodium Orthophosphate: Paddle-Wheel Mechanism Redefined in View of New Experimental Results. *Z. Phys. Chem.* **2000**, *214*, 643–673.
- (16) Andersen, N. H.; Bandaranayake, P. W. S. K.; Careem, M. A.; Dissanayake, M. A. K. L.; Wijayasekera, C. N.; Kaber, R.; Lundén, A.

Mellander, B.-E.; Nilsson, L.; Thomas, J. O. Paddle-Wheel versus Percolation Mechanism for Cation Transport in Some Sulphate Phases. *Solid State Ionics* **1992**, *57*, 203–209.

(17) Klarbring, J.; Simak, S. I. Phase Stability of Dynamically Disordered Solids from First Principles. *Phys. Rev. Lett.* **2018**, *121*, 225702.

(18) Zhu, Z.; Chu, I.-H.; Deng, Z.; Ong, S. P. Role of Na<sup>+</sup> Interstitials and Dopants in Enhancing the Na<sup>+</sup> Conductivity of the Cubic Na<sub>3</sub>PS<sub>4</sub> Superionic Conductor. *Chem. Mater.* **2015**, *27*, 8318–8325.

(19) Bo, S.-H.; Wang, Y.; Ceder, G. Structural and Na-Ion Conduction Characteristics of Na<sub>3</sub>PS<sub>4</sub>Se<sub>4-x</sub>. *J. Mater. Chem. A* **2016**, *4*, 9044–9053.

(20) Blachnik, R.; Rabe, U. Das Thermische Verhalten Der Mischungen Na<sub>2</sub>S-P<sub>4</sub>S<sub>10</sub> Und Na<sub>4</sub>Ge<sub>4</sub>S<sub>10</sub>-P<sub>4</sub>S<sub>10</sub> Des Systems Na<sub>2</sub>S-GeS<sub>2</sub>-P<sub>4</sub>S<sub>10</sub>. *Z. Anorg. Allg. Chem.* **1980**, *462*, 199–206.

(21) Takeuchi, S.; Suzuki, K.; Hirayama, M.; Kanno, R. Sodium Superionic Conduction in Tetragonal Na<sub>3</sub>PS<sub>4</sub>. *J. Solid State Chem.* **2018**, *265*, 353–358.

(22) Feng, X.; Chien, P.-H.; Zhu, Z.; Chu, I.-H.; Wang, P.; Immediato-Scuotto, M.; Arabzadeh, H.; Ong, S. P.; Hu, Y.-Y. Studies of Functional Defects for Fast Na-Ion Conduction in Na<sub>3-y</sub>PS<sub>4-x</sub>Cl<sub>x</sub> with a Combined Experimental and Computational Approach. *Adv. Funct. Mater.* **2019**, *29*, 1807951.

(23) Krauskopf, T.; Muy, S.; Culver, S. P.; Ohno, S.; Delaire, O.; Shao-Horn, Y.; Zeier, W. G. Comparing the Descriptors for Investigating the Influence of Lattice Dynamics on Ionic Transport Using the Superionic Conductor Na<sub>3</sub>PS<sub>4-x</sub>Se<sub>x</sub>Q. *J. Am. Chem. Soc.* **2018**, *140*, 14464–14473.

(24) Moon, C. K.; Lee, H.-J.; Park, K. H.; Kwak, H.; Heo, J. W.; Choi, K.; Yang, H.; Kim, M.-S.; Hong, S.-T.; Lee, J. H.; Jung, Y. S. Vacancy-Driven Na<sup>+</sup> Superionic Conduction in New Ca-Doped Na<sub>3</sub>PS<sub>4</sub> for All-Solid-State Na-Ion Batteries. *ACS Energy Lett.* **2018**, *3*, 2504–2512.

(25) Chu, I.-H.; Kompella, C. S.; Nguyen, H.; Zhu, Z.; Hy, S.; Deng, Z.; Meng, Y. S.; Ong, S. P. Room-Temperature All-Solid-State Rechargeable Sodium-Ion Batteries with a Cl-Doped Na<sub>3</sub>PS<sub>4</sub> Superionic Conductor. *Sci. Rep.* **2016**, *6*, 33733.

(26) De Klerk, N. J. J.; Wagemaker, M. Diffusion Mechanism of the Sodium-Ion Solid Electrolyte Na<sub>3</sub>PS<sub>4</sub> and Potential Improvements of Halogen Doping. *Chem. Mater.* **2016**, *28*, 3122–3130.

(27) Tanibata, N.; Noi, K.; Hayashi, A.; Tatsumisago, M. Preparation and Characterization of Highly Sodium Ion Conducting Na<sub>3</sub>PS<sub>4</sub>-Na<sub>4</sub>Si<sub>4</sub>S<sub>4</sub> Solid Electrolytes. *RSC Adv.* **2014**, *4*, 17120–17123.

(28) Tanibata, N.; Noi, K.; Hayashi, A.; Kitamura, N.; Idemoto, Y.; Tatsumisago, M. X-Ray Crystal Structure Analysis of Sodium-Ion Conductivity in 94 Na<sub>3</sub>PS<sub>4</sub>·6 Na<sub>4</sub>Si<sub>4</sub>S<sub>4</sub> Glass-Ceramic Electrolytes. *ChemElectroChem* **2014**, *1*, 1130–1132.

(29) Wu, E. A.; Kompella, C. S.; Zhu, Z.; Lee, J. Z.; Lee, S. C.; Chu, I.-H.; Nguyen, H.; Ong, S. P.; Banerjee, A.; Meng, Y. S. New Insights into the Interphase between the Na Metal Anode and Sulfide Solid-State Electrolytes: A Joint Experimental and Computational Study. *ACS Appl. Mater. Interfaces* **2018**, *10*, 10076–10086.

(30) Maekawa, H.; Matsuo, M.; Takamura, H.; Ando, M.; Noda, Y.; Karahashi, T.; Orimo, S. Halide-Stabilized LiBH<sub>4</sub>, a Room-Temperature Lithium Fast-Ion Conductor. *J. Am. Chem. Soc.* **2009**, *131*, 894–895.

(31) Sadikin, Y.; Schouwink, P.; Brighi, M.; Łodziana, Z.; Černý, R. Modified Anion Packing of Na<sub>2</sub>B<sub>12</sub>H<sub>12</sub> in Close to Room Temperature Superionic Conductors. *Inorg. Chem.* **2017**, *56*, 5006–5016.

(32) Yoshida, K.; Sato, T.; Unemoto, A.; Matsuo, M.; Ikeshoji, T.; Udovic, T. J.; Orimo, S. Fast Sodium Ionic Conduction in Na<sub>2</sub>B<sub>10</sub>H<sub>10</sub>-Na<sub>2</sub>B<sub>12</sub>H<sub>12</sub> Pseudo-Binary Complex Hydride and Application to a Bulk-Type All-Solid-State Battery. *Appl. Phys. Lett.* **2017**, *110*, 103901.

(33) Brighi, M.; Murgia, F.; Łodziana, Z.; Schouwink, P.; Wolczyk, A.; Cerny, R. A Mixed Anion Hydroborate/Carba-Hydroborate as a Room Temperature Na-Ion Solid Electrolyte. *J. Power Sources* **2018**, *404*, 7–12.

(34) Lundén, A. Enhancement of Cation Mobility in Some Sulphate Phases Due to a Paddle-Wheel Mechanism. *Solid State Ionics* **1988**, *28–30*, 163–167.

(35) Jansen, M. Volume Effect or Paddle-Wheel Mechanism - Fast Alkali-Metal Ionic Conduction in Solids with Rotationally Disordered Complex Anions. *Angew. Chem., Int. Ed. Engl.* **1991**, *30*, 1547–1558.

(36) Zhao, Q.; Pan, L.; Li, Y.-J.; Chen, L.-Q.; Shi, S.-Q. Rotational Motion of Polyanion versus Volume Effect Associated with Ionic Conductivity of Several Solid Electrolytes. *Rare Met.* **2018**, *37*, 497–503.

(37) Nilsson, L.; Thomas, J. O.; Tofield, B. C. The Structure of the High-Temperature Solid Electrolyte Lithium Sulphate at 908K. *J. Phys. C: Solid State Phys.* **1980**, *13*, 6441–6451.

(38) Tang, W. S.; Unemoto, A.; Zhou, W.; Stavila, V.; Matsuo, M.; Wu, H.; Orimo, S. I.; Udovic, T. J. Unparalleled Lithium and Sodium Superionic Conduction in Solid Electrolytes with Large Monovalent Cage-like Anions. *Energy Environ. Sci.* **2015**, *8*, 3637–3645.

(39) Meilander, B.-E.; Nilsson, L. Thermal Expansion of Lithium Sulphate. *Z. Naturforsch., A: Phys. Sci.* **1983**, *38*, 1396.

(40) Lundén, A. Evidence for and against the Paddle-Wheel Mechanism of Ion Transport in Superionic Sulphate Phases. *Solid State Commun.* **1988**, *65*, 1237–1240.

(41) Forland, T.; Krogh-Moe, J.; Moutschen-Dahmen, M.; Noer, B.; Reio, L. The Structure of the High Temperature Modification of Lithium Sulfate. *Acta Chem. Scand.* **1957**, *11*, 565–567.

(42) Michils, A. La Plasticité d'un Groupe Particulier de Cristaux Organiques. *Bull. Soc. Chim. Belg.* **1948**, *57*, 575–617.